Spectrally programmable light engine for *in vitro* or *in vivo* molecular imaging and spectroscopy

Nicholas MacKinnon, Ulrich Stange, Pierre Lane, Calum MacAulay, and Mathieu Quatrevalet

A spectrally and temporally programmable light engine can create any spectral profile for hyperspectral, fluorescence, or principal-component imaging or with medical photonics devices employing spectroscopy, microscopy, and endoscopy. Multispectral imaging feasibility was demonstrated by capturing nine images at wavelengths from 450 to 650 mm (25-nm FWHM) with a CCD-camera-equipped bronchoscope coupled to the light engine. Selected wavelength regions were combined to produce a color endoscopy image.

OCIS codes: 170.0170, 230.6120, 220.1770.

1. Introduction

Optical methods of detecting and diagnosing disease have been used by people throughout history,[1] but it is only since we have developed our understanding of the molecular basis of disease that we understand why. Because light interacts directly at the molecular level by absorption, fluorescence,[2] and other processes, and is also affected by the macrostructure and microstructure of tissue, which can cause scattering[3] and birefringence effects, it is a useful way of detecting changes in tissue. Whether it is a subtle change in tissue observed by an experienced endoscopist[4] or the first flush of fever observed by the parent of a child, the ability to detect these changes depends on the qualities of the light illuminating the tissue. Advances in genomics, proteomics, and molecular biology have led to new optical tools to detect subtle early changes in tissue that can allow early diagnosis and intervention.[5] Both *in vivo* and *in vitro* techniques exist that measure light transmission, reflectance, or the fluorescence of natural and artificial optical biomarkers, in both imaging and spectroscopy devices.[6]

The common thread of all optical and photonic technologies used in these devices is that they require illumination, often comprising highly specific wavelengths, to interact with tissues, biomarkers, or the chemical reagents in use for microplate or microarray[7] analyzers. Common methods to control the wavelength and intensity of light in these devices include the use of various types of lamps in combination with diffraction-grating monochrometers, filter wheels, shutters, apertures, and irises. These can impose a number of constraints on the types of tests or measurements instruments can perform. Limitations in possible wavelengths and speed of switching constrain automated optical analyzers such as microplate readers or clinical chemistry instruments. Inability to control illumination characteristics also limits the ability of endoscopy and minimally invasive surgical devices to differentiate tissue more effectively.[8] To answer this need, our group has developed a spectrally programmable light engine (SPLE) based on a Texas Instruments digital micromirror device,[9] or DMD, that can output arbitrary spectral profiles (Figs. 1–3).

2. Apparatus and Methods

The spectrally programmable light engine uses the DMD, in combination with a lamp and related optics, to control the wavelength-dependent energy distribution of light. The Texas Instruments DMD is a type of spatial light modulator most commonly found in digital image projection systems and projection televisions. In imaging applications, each mirror of the DMD is mapped to a pixel in a digital image. In current versions of the device, each mirror is

N. MacKinnon (nmackinn@bccrc.ca), U. Stange, P. Lane, and C. MacAulay are with the Cancer Imaging Department, British Columbia Cancer Research Centre, 601 West 10th Avenue, Vancouver V5Z1L3, British Columbia, Canada. M. Quatrevalet is with Ecole Superieure d'Optique, Institute d'Optique, Centre Universitaire, bât 503, 91403 Orsay cedex, France.

Received 20 July 2004; revised manuscript received 13 December 2004; accepted 7 January 2005.

0003-6935/05/112033-08$15.00/0

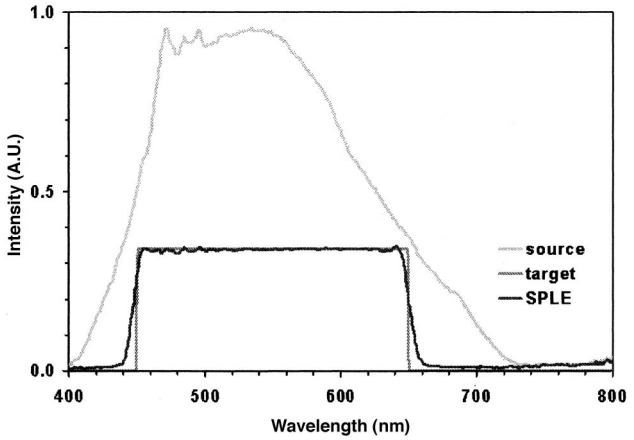

Fig. 1. Spectral flattening. The SPLE is used to shape the white-light spectrum of a xenon lamp (light gray) to approximate a spectrally flat target spectrum (dark gray). The measured SPLE output spectrum is shown in black.

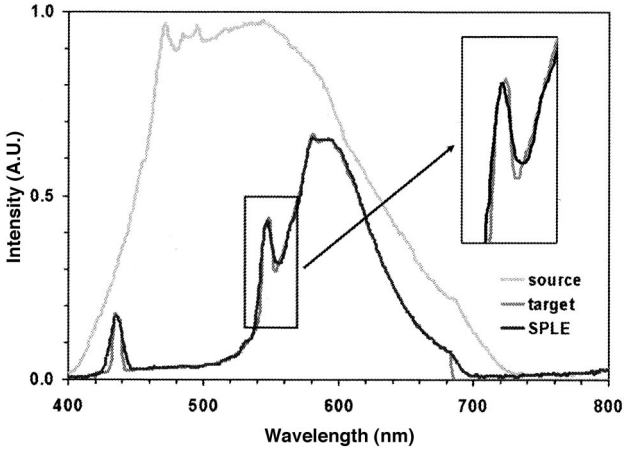

Fig. 3. Spectral profiling. The SPLE is used to shape the white-light spectrum of a xenon lamp (light gray) to mimic the spectrum of a fluorescent light source (dark gray). The measured SPLE output spectrum is shown in black. The inset box shows a detail of the target and measured spectra.

$\sim$12.6 μm square and spaced on 13.7-μm centers.[10] A typical array of 1280 by 1024 pixels is $\sim$17.5 mm in the long dimension. The mirrors are supported on a center post and tilt through plus or minus 12° from the normal by electrostatic attraction.

The spectrally programmable light engine (Fig. 4) optically disperses the white light from a lamp, LED, or fiber source, using a diffraction grating or prism, and images the spectrum onto the DMD mirror array. The emanating light can then be collected, focused, and mixed back together by spatial homogenization for use as the light source for an endoscopy, microscopy, or spectroscopy system or a scientific measurement system. The computer-controlled mirrors can be switched on and off at high speed (up to 20 kHz) to change the wavelength distribution of the light reflecting from the mirror array.

The optical designs we investigated for the SPLE were based on typical spectrograph designs.[11,12] One of the systems we built (Fig. 4) is constructed with a xenon arc lamp equipped with a spherical reflector and a condenser lens that focuses light onto an adjustable slit. Light from the slit is collected by a collimating lens and directed through a prism and an imaging lens to the DMD, where the image of the slit is dispersed across the DMD as a spectrum. The mirrors of the DMD are programmed to select which wavelengths and how much of each wavelength will be reflected to the collection lens. The collection lens focuses the light onto a spatial homogenizer and an integrating bar or other light guide.

We have investigated and constructed both prism- and diffraction-grating-based systems. Diffraction-grating systems have the benefit of linear wavelength dispersion but have the disadvantage of increased losses, especially at wavelengths further away from the blaze wavelength of the grating where diffraction efficiency is reduced. Prism systems have higher throughput across the spectrum, but nonlinear dispersion. When creating output spectra with a prism-based system, the number of wavelength axis pixels required to create an equivalent bandpass increases at the longer wavelength end of the spectrum (Fig. 5).

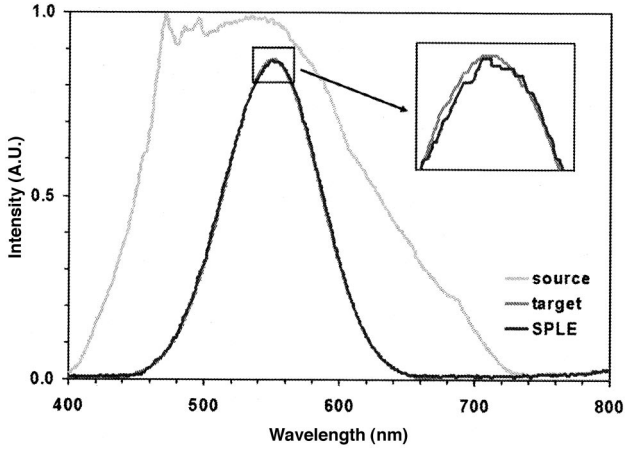

Fig. 2. Spectral shaping. The SPLE is used to shape the white-light spectrum of a xenon lamp (light gray) to approximate a Gaussian target spectrum (dark gray). The measured SPLE output spectrum is shown in black. The inset box shows a detail of the target and measured spectra.

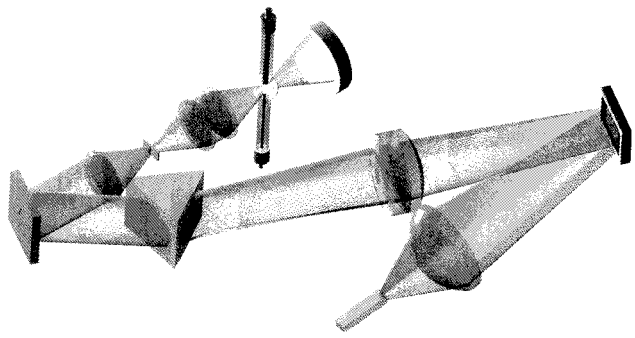

Fig. 4. Pictorial representation of key optical components of the SPLE in slit configuration (without anamorphic concentrator).

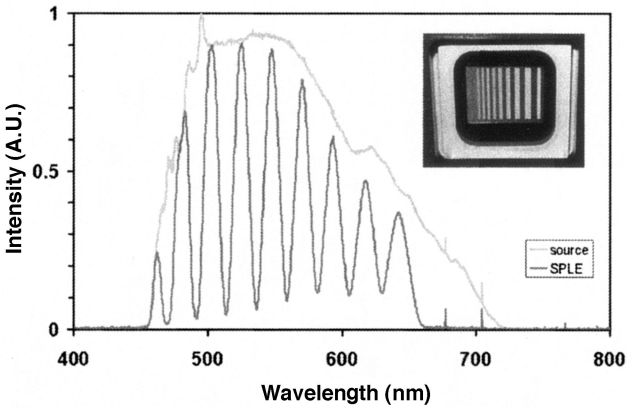

Fig. 5. Prism-based SPLE spectrum. A graph of the spectral output from a prism-based system showing the unequal DMD pixel mirror selection required (inset photograph) to produce the approximately equal output bandwidths in the spectrum.

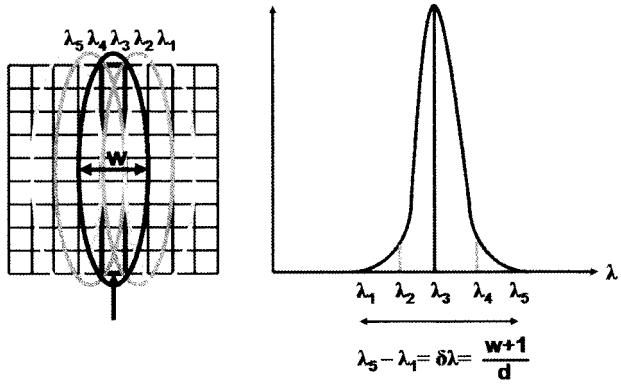

Fig. 6. Spectral resolution. On the left, a section of a DMD is shown schematically with a number of slit images imaged onto pixel columns. On the left, the spectral intensity distribution of the light impinging on the pixel mirror column marked with an arrow is shown schematically.

In most spectrographs, the light to be analyzed is directed through a pinhole or slit, and then the plane of this pinhole or slit is imaged onto the plane of a detector, usually a CCD. A dispersing element is positioned in the optical chain, providing a plurality of images of the slit, each corresponding to a discrete wavelength range, and spread along the axis of spectral dispersion. The ratio between the size of the image of the pinhole or slit along this axis and the dispersive power of the system determines the spectral resolution of the spectrograph. However, the size of the pinhole or the slit also determines the amount of light that actually goes through the system, and this is where the most important challenge lies in the design of spectrographs: to find the right compromise between resolution and sensitivity.

The same situation applies for the spectrally programmable light source; the aim is to image a tall and narrow line of light onto the rectangular DMD. The spectral resolution $\delta\lambda$ is determined by the bandwidth of wavelengths that falls onto a single column of micromirrors, and this bandwidth is in turn determined by the width w (in pixels) of the image of the slit for a single wavelength, combined with the dispersive power d of the system (in pixels per nanometer) (Fig. 6):

$$\delta\lambda = (w + 1)/d.$$

For a light source with a spectral range covering 400–700 nm, a spectral resolution of 10 nm, and with a DMD that is 17.5 mm in the wavelength axis, the image of the bar of light must be ~0.6 mm wide. The $\pm 12°$ tilt of the DMD mirrors constrains the optical design of a DMD light source to $\sim f/2.3$.[9] Unlike a spectrometer where light striking the detector is converted to a signal and does not continue to propagate, the light striking the DMD must be deflected to an exit path. The relatively small tilt of the DMD mirrors means that any image (including a spectrum) has to be projected with a low numerical aperture (NA). Larger numerical apertures will result in angles of illumination striking the DMD mirrors that exceed the angles that can be deflected along the output path. This limitation in turn constrains the numerical aperture of the system, placing significant constraints on conventional optical methods to focus a light source to a narrow line.

Illumination spectra were measured with a calibrated spectrometer (Ocean Optics USB-2000), and endoscopic images were captured with an Olympus BF-10 bronchoscope and a CCD camera (Andor Technologies model DV885 DCF-VP). Integration times for image capture varied as a function of illumination intensity and ranged from ~10 ms to 100 ms, or approximately from 1/3 to 3 times video rate.

Measurements of out-of-band rejection were made with a calibrated USB-2000 spectrometer coupled to an integrating sphere, and with signal measurement performed at 100-ms integration time and the low-level out-of-band signal measured at 10,000-ms integration time.

Low-level control of the on–off state of the DMD mirrors was accomplished by a custom driver using a dynamic link library that communicated with the DMD controller. The overall control software for the SPLE was written in the graphical programming language LabVIEW (National Instruments), using functions that called the dynamic link library, which interacted directly with the DMD controller and the feedback spectrometer. These functions provided dynamic feedback from the intensity-calibrated spectrometer, which obviated the need to do intensity calibration of the SPLE. Since the SPLE can only attenuate the light from the primary source, the maximum output will be the maximum intensity of the source modified by the optical transfer function of the grating or prism, system optics, and DMD.

3. Discussion and Results

We have constructed several systems that use slits to constrain the input illumination to a narrow line of

light. However, if we use a slit to create the narrow line, we lose a great deal of light, since the slit works as a stop preventing photons from propagating. High-power light sources with parabolic or elliptical reflectors or condenser lens systems all face the problem of the law of conservation of the geometric étendue. What is gained on one side (a higher density of energy in the focal plane of the condenser) is lost on the other side (a more diverging beam). If larger numerical aperture optics are used to focus the beam onto the slit, then larger numerical aperture optics will be needed to collimate the beam before directing it into the spectral dispersion element. Since the angle of deflection of the DMD constrains the numerical aperture of optical elements that image the spectrum onto the DMD, the mismatch in NA results in spectrum image magnifications that are not likely to be suitable for most applications that require spectral resolving power but may be an advantage for some that do not. Examples of lower-resolution applications where total energy might be more important and this magnification could be used effectively include RGB (red-green-blue) imaging, or white-light color balancing. However, many applications do require better wavelength control and better resolution.

An interesting fact needs to be noted though: only the size of the slit along the spectral axis is of interest for the resolution. From this simple fact, Davidson *et al.*[13] imagined an original solution for the étendue problem: an anamorphic transformation of the input light using a pair of cylindrical lenses and a Porro prism array. There are a host of efficiency problems with using a prism array for such a task, and so we first decided to try to improve the refractive array by optimizing the angles of the prism, resulting in some efficiency improvements, but finally decided to develop a new all-reflective optical element for this task. Unlike the Porro prism in a binocular where all light travels at angles close to the axis of propagation, the light converging on the prism array in a SPLE has a greater angular distribution. Since the angle of total internal reflection varies with wavelength and with angle of incidence, the angular distribution of our illumination resulted in some light not meeting the criteria for total internal reflection and thus reducing the efficiency of the prism array. Switching to a reflective element eliminates this issue, since we no longer rely on total internal reflection.

In our implementation of this (Figs. 7–10), a collimated beam of light is focused with a cylindrical lens into a vertical bar of light. In the focal plane of the cylindrical lens, the light is collimated in one axis and converging or diverging in the other axis. By placing a suitable micro-optical array (Fig. 8) in the focal plane, it is possible to piecewise exchange the converging and collimated axes. As the beam is reflected, each element of the array rotates the two axes of a small portion of the vertical bar of light through 90°, resulting in a bar of light that is now diverging in the long dimension and collimated in the narrow dimension. This is accomplished by two

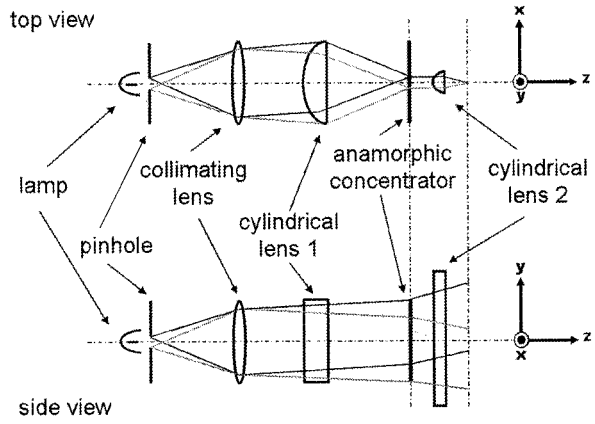

Fig. 7. Schematic representation of the anamorphic concentrator. Cylindrical lens 1 focuses the collimated light beam onto the anamorphic concentrator. The sharpness of the focus depends on the size of the pinhole. The concentrator exchanges the noncollimated axis (x axis) and the collimated axis (y axis). The resultant beam is focused again by cylindrical lens 2, resulting in a loss of focus in the previous collimated axis but sharper focus in the previous noncollimated axis. The resulting image of the pinhole is a narrowly focused line.

successive 45° rotations at each reflection from the mirror surface. This collimated beam can in turn be focused again by a second cylindrical lens into an even narrower line that can then be imaged onto a spectrograph or the DMD of a spectrally programmable light engine. No light has been lost because no physical aperture has been used, and the product (beam size) × (angular size) is constant in accordance with conservation of the geometrical étendue. The design of this key enabling element that has allowed us to produce this spectrally programmable light engine will be treated in detail in another paper. During the course of developing the SPLE, we made extensive use of Zemax (Zemax Development Corporation, San Diego, California) optical modeling software. To assess the optical efficiency and wavelength resolution of our designs, we modeled a system with a reflection prism array in Zemax's sequential mode

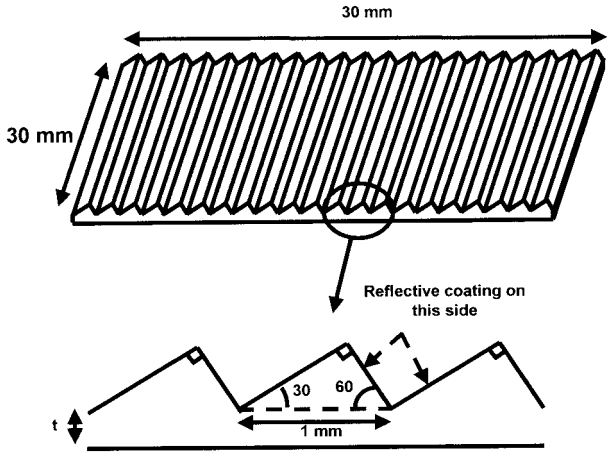

Fig. 8. Microprism array with inset showing angles of facets.

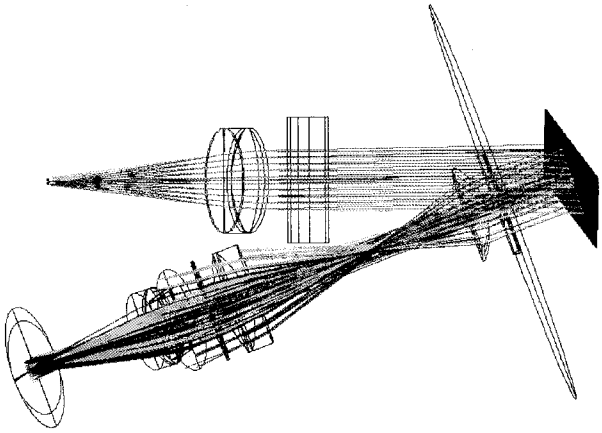

Fig. 9. Optical system with anamorphic concentrator modeled in Zemax showing three-dimensional layout of components.

(Fig. 9). The technique for simulating the Cermax lamp is to use the "geometrical image analysis" feature with the "circle" shape and a size for the field that corresponds roughly with the size of the pinhole from our nonsequential model of the source, and a power that corresponds with the one measured using the nonsequential model of the Cermax lamp for this given aperture. With an additional cylindrical lens so that the y dimension of the image fits with the size of the DMD, and a 4-mm pinhole that passes 13 W, the detector image (Fig. 10) is 17 mm by 17 mm. Focal lengths of the cylindrical lenses along the y direction are as follows: the first one in the optical path is $F = 60$, $D = 40$; the second one is $F = 190$, $D = 30$.

The white rectangle on the detector (shown for scaling purposes) is 15 mm by 10 mm. These model images show the spectral resolution that can be theoretically achieved with this nonimaging optical method of creating a "virtual slit." Each vertical line illustrates the dispersion and loss of resolution of the ideal pure wavelength generated in the source. The 12 lines shown are from 400 to 730 nm in 30-nm increments.

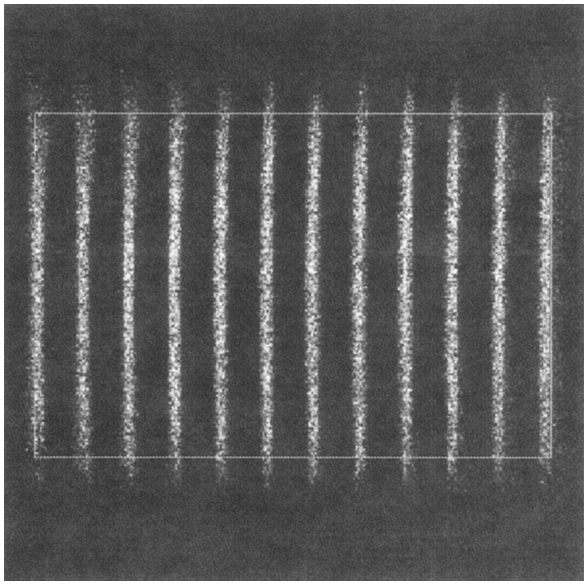

Fig. 10. Optical system with anamorphic concentrator modeled in Zemax showing detector image of a dispersed spectrum from a theoretical source with 12 perfect spectral lines at 30-nm intervals from 400 to 720 nm.

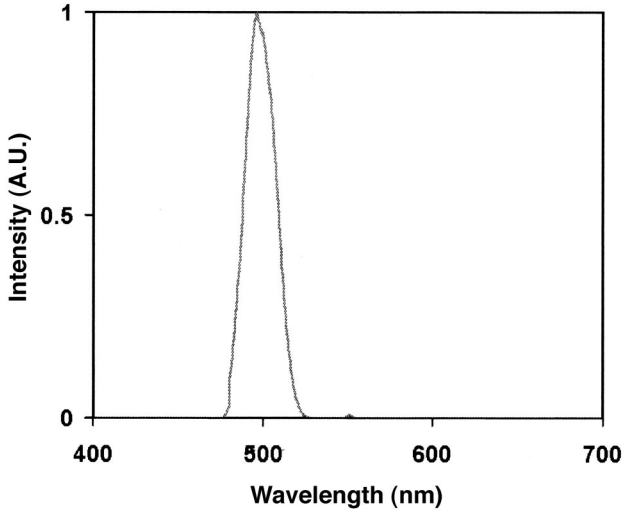

Fig. 11. Spectrum of 28-nm FWHM bandpass output with center wavelength of 500 nm. Nine such spectral shapes centered at 450, 475, 500, 525, 550, 575, 600, 625, and 650 nm were used to acquire the multispectral endoscope images in Fig. 13.

The light reflecting along the beam propagation path from the DMD must be collected, focused, and spatially homogenized. There are a number of methods to spatially homogenize light, including diffusers, light-shaping diffusers, integrating spheres, and light guides. For our initial studies, the light was simply focused into a liquid light guide for homogenization. The output from the liquid light guide was directed into an integrating sphere coupled to the spectrometer to measure the spectral composition and enable feedback control of the light engine.

Performance of light sources is defined by output power, spectral shape, and spectral range. Performance of optical filters is defined by wavelength range, optical efficiency, steepness of cut-on or cut-off (sometimes referred to as Q factor), and out-of-band rejection. The same parameters can be applied to the SPLE. The broadband output power 420–680 nm measured from a liquid light guide connected to the SPLE connected was 100 mW for a 100-W xenon arc lamp source and at 20 mW for a 200-W mercury–xenon arc lamp source. The cut-on and cut-off frequency is steep and is comparable to slopes achievable with interference filters, but without the ripple or "ringing" commonly observed with those filters (Fig. 11). Out-of-band rejection is important for many imaging applications and for fluorescence applications. With a DMD-based system, the ability of the mirror array system to "turn off" undesirable wavelengths is what determines the out-of-band rejection. Some photons will be diffusely reflected from the nonmirrored portions of the DMD between the

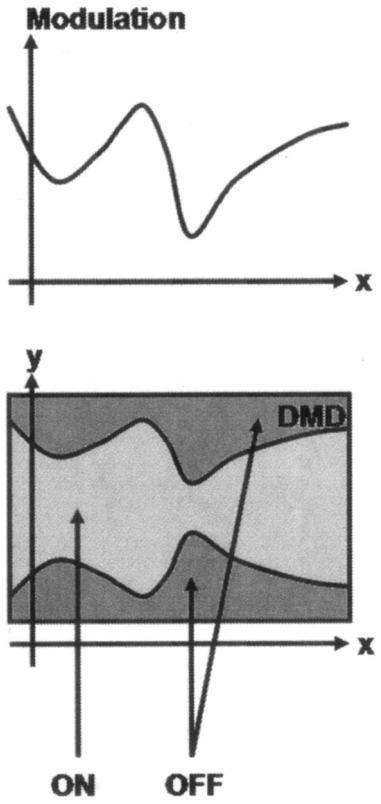

Fig. 12. Diagram illustrating how the intensity modulation of a range of wavelengths can be selected by the equivalent on–off state of mirrors distributed spatially around wavelength axis positioned at the center row of mirrors on the DMD.

movable mirrors, and some photons will be scattered by mirror edges and other irregularities. The native contrast (largely determined by diffraction or stray light reflections from the mirror elements) of the DMD is specified as 1000:1 or OD3.[6] Spectral measurements showed an out-of-band rejection ratio of 756:1 at 550 nm when the SPLE is set to 450-nm illumination (15-nm FWHM) on our benchtop setup. If a single DMD is used, then optical strategies such as stops, polarizers, and baffles can be put in place to somewhat improve contrast for fluorescence applications. The small NA of the system is helpful for this. If two DMD surfaces are used in sequence, with the spectrum reimaged onto the second DMD surface before passing the light onto the output, contrast ratios of 500 000 are possible, although optical efficiency drops by 30%.

Once we have a spectrum of suitable intensity and resolution imaged onto the DMD spatial light modulator, tuning the spectrum is a simple function of turning on or off the appropriate mirrors. Just as the number of pixels in a row determines the wavelength resolution, the number of pixels in a column determines the intensity distribution at the wavelength the column represents. As shown in Fig. 12, the mirrors in a column can be switched off symmetrically around the wavelength axis positioned at the center row of mirrors on the DMD to adjust the intensity of illumination. Other modes of controlling intensity are possible, such as selecting the mirrors to be turned off according to the intensity distribution in a column of mirrors, or modulation by rapidly turning mirrors on and off. Adjusting a range of columns by any of these methods can shape a spectrum.

We developed an algorithm that reads any arbitrary spectrum from a tab-delimited text file and then adjusts it so that the intensities of the desired spectrum at all its wavelengths fit optimally within the maximum available intensity of the calibrated output of the white-light source. The program then iteratively measures the output spectrum, calculates the differences in intensity between the measured spectrum and the target spectrum at each wavelength, and then adjusts the number of mirrors that are turned on or off in each column until the program converges on an output it cannot improve. In this way, any spectrum within the limits of resolution of the device can be created. Figures 1–3 show examples of spectral flattening, creation of a Gaussian spectral profile, and reproduction of a measured spectrum (in this case the ceiling-fixture fluorescent tubes of our laboratory as measured by the USB-2000 spectrometer). The fluorescent lamp profile, Fig. 3, is interesting because is shows the limits of the optical resolution of the system (and to some degree our algorithms). To prevent resonance in the feedback system, we adjusted the spectrum in blocks that were 5 nm wide. Since the pixel columns cover a much narrower wavelength range than the optical resolution of the spectral dispersion system, adjusting a single column of mirrors affects the spectral content over a wider range than its nominal value (as explained in Fig. 6). For example, a spectral range of 400–700 nm spread over 1024 pixel columns results in a spectral range of 0.3 nm per pixel column; this is much narrower than any practically usable slit width of the order of hundreds of nanometers. More sophisticated algorithms that take this optical resolution profile into account should allow us to produce improved feedback control. Once a spectral profile is defined, the mirror pattern can be stored as a template and recalled.

As a first-order test of feasibility for endoscopy applications, we butt-coupled the liquid light guide to an Olympus BF-10 bronchoscope and used it to successfully view tissue, in this case a closed hand simulating a bronchial passage, under white-light illumination. We also sequentially applied red, green, and blue light via the SPLE and were able to distinguish tissue features for all three wavelength ranges. We further connected a CCD camera to the bronchoscope and captured multispectral images of the tissue for a sequence of nine wavelength bands (Fig. 11 shows an example) at 25-nm increments from 450 to 650 nm and at a FWHM bandpass of 28 nm. These 16-bit gray-scale images were scaled to provide equivalent dynamic range and converted to 8-bit images (Fig. 13). Three of these images were combined and scaled to create an RGB image (Fig. 14) that would be typical of the type of image an endoscopist would see.

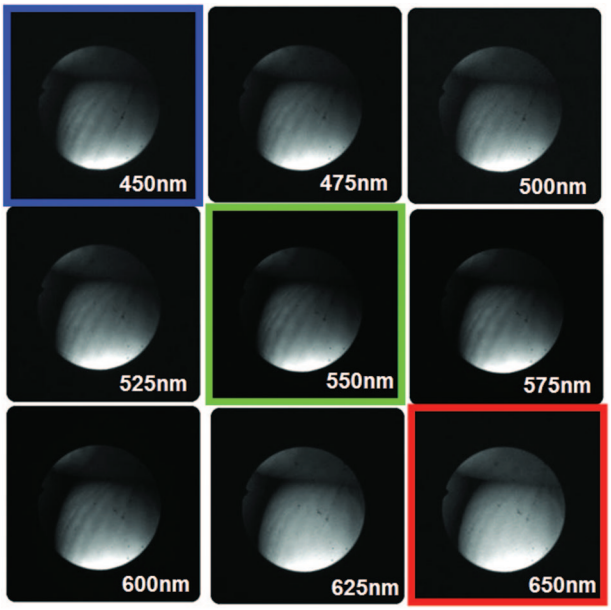

Fig. 13. Nine multispectral images acquired of tissue with Olympus P-10 bronchoscope coupled through C-mount ocular adapter with CCD camera under SPLE illumination shown in Fig. 11.

The dynamic control of this light source would allow endoscopists to view tissue in conventional imaging modes such as sequential or simultaneous RGB capture. Additionally, the dynamic range of most existing endoscopes can be enhanced by high-speed digital control of the light. Digital illumination information can be combined with digital imaging information in a bit additive mode, e.g., 8-bit control of illumination intensity could be combined with 8-bit sensitivity of a CCD to provide 16-bit imaging. This will allow small-well CCDs typically found in "chip on the tip" endoscopes to avoid saturation more deftly.

More advanced applications of this illumination technique could include quickly switching to multispectral or hyperspectral imaging at a site of interest to provide enhanced diagnostic information, or inputting a spectral profile that produces enhanced contrast for a particular anatomical feature or pathology.

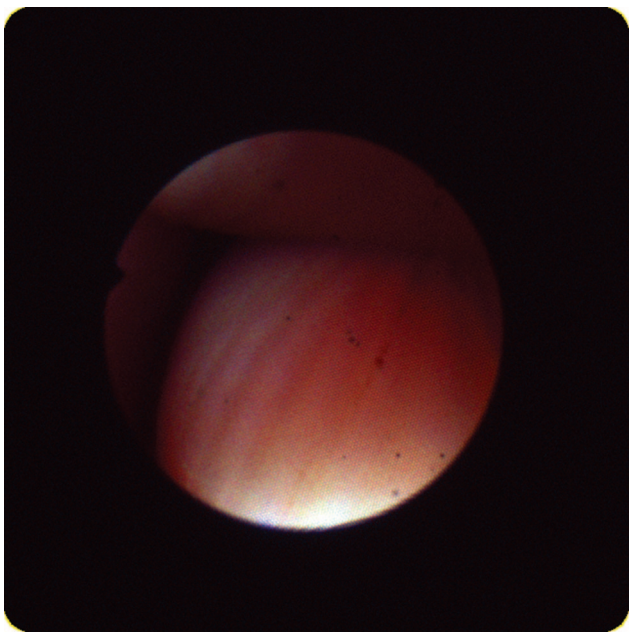

Fig. 14. Color image (RGB) synthesized from 450-, 550-, and 650-nm monochrome multispectral bronchoscope images shown in Fig. 13 acquired with CCD camera and SPLE illumination shown in Fig. 11.

4. Conclusions and Future Research

A spectrally tunable light engine with dynamic feedback control has been demonstrated. The SPLE can reproduce or create a range of spectral profiles, including those suitable for RGB video imaging with monochrome sensors. With a switching time of 20 kHz, it can step through thousands of spectral profiles in a few seconds, which may make it useful for rapid analysis in field spectroscopy and hyperspectral imaging applications. Its ability to replace filters, filter wheels, or filter changers and shutters may make it suitable for a host of life and analytical science applications. Use of this light source for endoscopic imaging has been demonstrated.

In future work, we plan to explore high out-of-band rejection configurations of the SPLE that will enable effective fluorescence applications. In the near term, we will be constructing hyperspectral microscopy systems and coupling the system to commercially available chip-on-tip color video endoscopes to test the ability to improve dynamic range and diagnostic ability with these endoscopes.

References

1. T. Vo-Dinh, "Biomedical photonics: a revolution at the interface of science and technology," in *Biomedical Photonics Handbook*, T. Vo-Dinh, ed. (CRC Press, Boca Raton, Fla., 2003), pp. 1.1–1.18.
2. B. Pogue and M. A. Mycek, eds., *Fluorescence in Biomedicine* (Marcel Dekker, New York, 2004).
3. V. Tuchin, "Light-tissue interactions," in *Biomedical Photonics Handbook*, T. Vo-Dinh, ed. (CRC Press, Boca Raton, Fla., 2003), pp. 3.1–3.26.
4. S. Lam, T. Kennedy, M. Unger, Y. Miller, D. Gelmont, V. Rusch, B. Gipe, D. Howard, J. LeRiche, A. Coldman, and A. F. Gazdar, "Localization of bronchial intraepithelial neoplastic lesions by fluorescence bronchoscopy," Chest **113,** 696–702 (1998).
5. T. Dixon, F. Dorn, P. Boulanger, H. Chrostowski, B. Dobson, L. Leonardi, T. Salcudean, B. Sawicka, and B. Wilson, "Emerging technologies with emphasis on photonics," Report of Working Group 5 of the Medical Imaging Technology Roadmap Steering Committee (Industry Canada, Ottawa, Canada, 2001).
6. T. Vo-Dinh, ed., *Biomedical Photonics Handbook* (CRC Press, Boca Raton, Fla., 2003).
7. M. Schena, *Microarray Analysis* (Wiley, New York, 2003).
8. E. Lindsley, E. S. Wachman, and D. L. Farkas, "The hyperspectral imaging endoscope: a new tool for *in vivo* cancer detection," in *Imaging, Manipulation, and Analysis of Biomolecules, Cells, and Tissues II*, D. V. Nicolau, J. Enderlein, R. C. Leif, and D. L. Farkas, eds., Proc. SPIE **5322,** 75–82 (2004).

9. L. J. Hornbeck, "Digital light processing for high brightness, high resolution applications," in *Projection Displays III*, Ming H. Wu, ed., Proc. SPIE **3013,** 27–40 (1997).
10. D. Dudley, W. Duncan, and J. Slaughter, "Emerging digital micromirror device (DMD) applications," Texas Instruments White Paper, Plano, Texas, Feb. 2003; available from www.dlp.com.
11. E. G. Loewen and E. Popov, *Diffraction Gratings and Applications* (Marcel Dekker, New York, 1997).
12. C. Palmer, *Diffraction Grating Handbook*, 4th ed. (Richardson Grating Laboratory, Rochester, New York, 2000).
13. N. Davidson, L. Khaykovich, and E. Hasman, "High resolution spectrometry for diffuse light by use of anamorphic concentration," Opt. Lett. **24,** 1835–1837 (1999).